Agricultural Water Management 318 (2025) 109678

Contents lists available at ScienceDirect

Agricultural Water Management

journal homepage: www.elsevier.com/locate/agwat

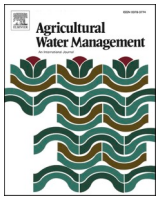

Strategies for mitigating winter wheat yield reduction in the Yellow River basin: Simulations and insights from CMIP6 data and the improved DSSAT-CERES-wheat model

Yingnan Wei [a,b], Ziya Zhang [c], Miaolei Hou [a], La Zhuo [b], Ning Yao [a,*], LinChao Li [d], Jiangfeng Xiangli [e], Tehseen Javed [f], Jianqiang He [a], Qiang Yu [b,*]

[a] College of Water Resources and Architectural Engineering/Key Lab of Agricultural Water and Soil Engineering of Education Ministry, Northwest Agriculture and Forestry University, Yangling, Shaanxi 712100, PR China
[b] College of Soil and Water Conservation Science and Engineering, Northwest Agriculture and Forestry University, Yangling, Shaanxi 712100, PR China
[c] Yellow River Engineering Consulting Co., Ltd, Institute of Planning Research, Zhengzhou 450003, China
[d] College of Agronomy, Inner Mongolia Agricultural University, Hohhot 010019, PR China
[e] Shaanxi Provincial Flood and Drought Disaster Prevention Center, Xi'an, Shaanxi 710004, PR China
[f] Department of Environmental Sciences, Kohat University of Science and Technology, Kohat 26000, Pakistan

ARTICLE INFO

Handling Editor - Dr R Thompson

Keywords:
Winter wheat
DSSAT-CERES-Wheat
Drought
Crop failure
Coping measures

ABSTRACT

Winter wheat is a vital staple crop in northern China, and climate change is expected to increase the frequency of droughts, leading to reduced yields. Therefore, it is crucial to study the impact of climate change on winter wheat yield and develop strategies to mitigate these effects. This study used CMIP6 data and an improved DSSAT-CERES-Wheat model to simulate winter wheat's phenological stages, yield, and water stress factors in the Middle and upper reaches of Yellow River basin from 2022 to 2050 and proposed measures to counteract yield reduction. The results revealed that optimal sowing dates and irrigation strategies remained stable under both the Shared Socioeconomic Pathway 2–4.5 (SSP2–4.5) and Shared Socioeconomic Pathway 5–8.5 (SSP5–8.5) scenarios across the middle and upper reaches of the Yellow River Basin. Early sowing combined with targeted irrigation during the jointing and grain-filling stages enhanced winter wheat yields but led to delayed phenological development. Moreover, variations in water productivity (WPc) and yield exhibited consistent spatial patterns across the three subregions of the study area. In region 1, the optimal sowing date is 10 days earlier, with a sowing window of 7–13 days earlier. During normal and dry years, irrigation requirements at the jointing and filling stages are 70 mm and 90 mm, respectively. In regions 2 and 3, the optimal sowing date is 15 days earlier, with a sowing window of 12–18 days earlier. Under the SSP2–4.5 and SSP5–8.5 scenarios, the overall growth rates of winter wheat yield in the Middle and upper reaches of Yellow River basin were 20.62 % and 16.32 %, respectively, with irrigation levels of 60 mm and 80 mm at the jointing and filling stages during normal and dry years. This study provides valuable insights and references for developing strategies to mitigate winter wheat yield reduction in the Middle and upper reaches of Yellow River basin under future climate scenarios.

1. Introduction

Wheat yield is a critical parameter for global food security, and winter wheat (*Triticum aestivum L.*) is extensively cultivated worldwide (Shiferaw et al., 2013). In China, winter wheat is primarily grown in the southwest, northwest, the Huang-Huai-Hai Plain, and the middle and lower reaches of the Yangtze River, contributing up to one-sixth of the global winter wheat output (Wu et al., 2022). In the Middle and upper reaches of Yellow River Basin, winter wheat is the most essential food crop, crucial for sustaining people's livelihoods (Long et al., 2022) and the contemporary economic development of the region. However, winter wheat growth in the Middle and upper reaches of Yellow River Basin faces challenges from climate change, rising temperatures, and increased drought events (Christian et al., 2021). Despite these challenges, uncertainty persists regarding how winter wheat will grow and develop under future drought conditions and which drought mitigation

* Corresponding authors.
E-mail addresses: yaoning@nwafu.edu.cn (N. Yao), yuq@nwafu.edu.cn (Q. Yu).

https://doi.org/10.1016/j.agwat.2025.109678
Received 8 January 2025; Received in revised form 12 July 2025; Accepted 16 July 2025
Available online 22 July 2025

strategies will be most effective. Therefore, forecasting winter wheat yields under future drought scenarios and developing appropriate response strategies are crucial for ensuring national food security and supporting economic development.

Various methods exist to assess the impact of drought on winter wheat yield, including field water control experiments (Gao et al., 2007), crop growth models (Bai et al., 2024; Rahimi-Moghaddam et al., 2021), and statistical analyses (Javed et al., 2021; Shi et al., 2024). However, each method has inherent limitations. Field water control experiments are limited by time and space, crop models often underperform under water stress, and statistical methods fail to fully reveal the processes and mechanisms of drought impacts on crops (Sun et al., 2021). To overcome these limitations, this study combines multiple methods and cross-validates results to reduce the uncertainty in drought impact assessments. This approach is crucial for reducing agricultural drought risk and ensuring food security.

Drought coping strategies have received widespread attention, with scholars proposing various approaches. These strategies can be categorized into four main groups: livelihood diversification, long-term livelihood strategies, short-term coping activities, and erosion coping strategies (Quandt, 2021). Farmers typically adapt to drought by adjusting crop varieties and planting dates and implementing water-saving and irrigation management practices (Li et al., 2015). Previous research has demonstrated that adjusting sowing dates in response to drought (Hu et al., 2017; Yang et al., 2019; Tu et al., 2022) and adopting rational irrigation practices (Mu et al., 2023; Liu et al., 2024) can enhance crop yields. However, few studies have investigated the combined effects of adjusting sowing dates and implementing irrigation practices on winter wheat in the arid and semi-arid regions of the middle and upper reaches of the Yellow River Basin.

Since the mid-20th century, drought-affected areas in the middle and upper reaches of the Yellow River Basin have shown a consistent annual expansion. Provinces including Gansu, Shaanxi, Henan, Shanxi, and Shandong have reported drought-impacted regions totaling up to 75,300 km^2, accounting for approximately 70 % of the nation's total drought-affected area. Crop losses in these regions can reach 90,000 km^2, with direct economic losses amounting to 6 billion yuan. These conditions seriously threaten the Yellow River Basin's economic development, food security, and ecological stability (Li et al., 2021). Notably, the middle reaches of the Yellow River, which are situated in arid and semi-arid ecologically fragile zones, are also critical areas for soil and water conservation efforts in China (Zhang et al., 2023). Therefore, quantitative assessments of drought impact on grain crops in the Middle and upper reaches of Yellow River Basin are valuable for maintaining the region's ecological and food security.

Considering the current drought conditions affecting winter wheat in the middle and upper reaches of the Yellow River Basin. In alignment with the region's sustainable development goals, an enhanced DSSAT-CERES-Wheat model was employed to simulate winter wheat's phenological development and yield from 2022 to 2050. The objective of this study were to (1) reveal the change in winter wheat growth and development under future climate and drought scenarios, (2) identify the optimal sowing times for achieving high yields of winter wheat in various regions of the Middle and Upper reaches of Yellow River basin, (3) explore the optimal growth stage of winter wheat under the optimal sowing dates and local irrigation quotas. These findings aim to establish the best sowing dates and irrigation strategies for maintaining high and stable winter wheat yields under climate change and drought conditions, providing a scientific basis for drought management and food security.

2. Materials and methods

2.1. Study area and data source

2.1.1. Study area

The middle and upper reaches of the Yellow River Basin originate in the Bayankala Mountains of Qinghai Province and flow from west to east through nine provinces and autonomous regions in China. This section of the basin encompasses 362 county-level administrative units and ultimately discharges into the Bohai Sea at Kenli County, Dongying City, Shandong Province. It traverses the first, second, and third topographic steps of China's terrain, extending approximately 5464 km in length and covering a basin area of about 795,000 km^2, with an internal flow area of roughly 42,000 km^2. The basin's geographical range lies between 95°53' to 119°05' E longitude and 32°10' to 41°50' N latitude, making it the second-longest river in China (Fig. 1). The climate in most parts of the Middle and upper reaches of Yellow River basin is characterized by a continental monsoon climate, with significant spatial variation due to topographic factors. Climatic conditions, such as precipitation and evaporation, vary greatly, with less rainfall and an uneven seasonal distribution. The western part of the basin tends to be drier, while the eastern part is wetter, with precipitation generally decreasing from southeast to northwest (Wang et al., 2020a). According to China's nine agricultural region classification standards, the Middle and upper reaches of Yellow River basin is divided into three distinct regions. Region 1 is located in the middle and upper reaches of the Yellow River basin, which is classified as an arid and semi-arid agricultural region in the north. Region 2 is situated in the upper reaches of the Middle and upper reaches of Yellow River basin, part of the Qinghai-Tibet Plateau. Region 3 is found in the lower reaches, which includes the Loess Plateau and the Huang-Huai-Hai Plain. Winter wheat cultivation varies across these regions, with fewer cultivation sites in Regions 1 and 2 and a higher concentration of sites in Region 3.

2.1.2. Data source

The CMIP6 data is part of the sixth Coupled Model Intercomparison Project (CMIP), organized by the World Climate Research Programme (WCRP). It provides a reliable reference for predicting future climate change using global climate models (GCMs) (Ma et al., 2024; Zhu et al., 2020). Compared to CMIP5, the ongoing CMIP6 models exhibit a lower degree of uncertainty in simulating precipitation and temperature, yield better results in extreme index changes, and offer improved applicability for future climate predictions across different climate models (Zhu et al., 2021; Jia et al., 2023).

This study selected two Shared Socioeconomic Pathways (SSP2–4.5 and SSP5–8.5) from the Coupled Model Intercomparison Project Phase 6

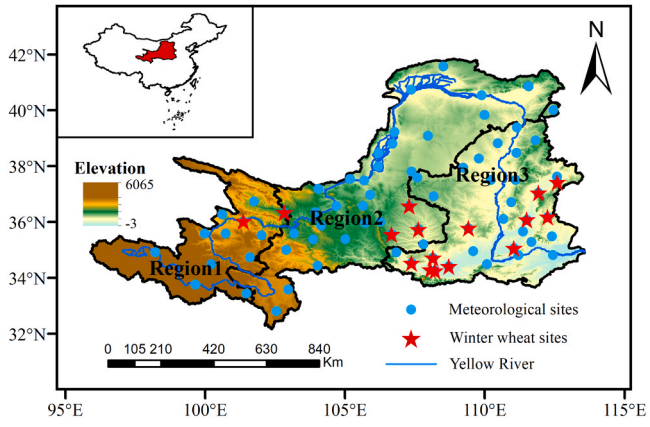

Fig. 1. Distribution map of meteorological stations, elevation, and winter wheat stations in the Middle and upper reaches of Middle and upper reaches of Yellow River basin.

(CMIP6) to predict future climate change in winter wheat-growing regions of the Middle and upper reaches of Yellow River basin from 2022 to 2050. The CMIP6 data were available through the CMIP6 global climate research plan (https://esgf-node.llnl.gov/search/cmip6/). The precipitation (P), maximum temperature (T_{max}), minimum temperature (T_{min}), solar radiation, and air pressure were downloaded from 27 different GCMs (Table S1) from 1961 to 2050.

Soil data, including soil moisture and physical parameters, were obtained through the Google Earth Engine (GEE) platform (https://code.earthengine.google.com/). The daily data of soil moisture content data at depths of 0–10 cm, 10–40 cm, 40–100 cm, and 100–200 cm from the GLDAS dataset, covering the years 1961–2021, were extracted for the station. Data on soil physical parameters, including bulk density, field capacity, and wilting coefficient, were sourced from the Cold and Arid Regions Science Data Center National Earth Science Data Platform (http://westdc.westgis.ac.cn/).

Phenological data for winter wheat, sampled from observation stations in the middle and upper reaches of the Yellow River Basin between 1992 and 2013, along with yield data collected from 2000 to 2013, were obtained from the China Meteorological Data Service Center. The growth cycle of winter wheat is classified into nine stages: sowing, emergence, overwintering, green-up, jointing, panicle formation, heading, flowering, and maturity. Winter wheat is sown between September and October and harvested the following June. The types, sources, and sampling details of all datasets used are summarized in Table 1.

2.2. Methods

2.2.1. Improved DSSAT-CERES-Wheat model

The DSSAT (Decision Support System for Agrotechnology Transfer) model, developed by the United States Department of Agriculture, is widely used for agricultural test analysis, yield forecasting, and agricultural production risk assessment. Known for its user-friendly interface and broad applicability, the DSSAT incorporates the CERES-Wheat model within the CSM (Crop System Model) platform (DSSAT v4.7) to simulate soil carbon and nitrogen dynamics, water balance, as well as wheat growth, development, and yield. To simulate crop growth and yield accumulation from sowing to harvest, the model requires inputs such as meteorological data, soil data, crop management data, and crop parameter data (Jones et al., 2003).

Table 1
Basic Data information.

Data Category	Description	Source
Basic geographic information data of the study area	Boundary, river, and elevation data.	National Data Center for Glaciology and Permafrost Desert Science (http://www.ncdc.ac.cn).
Meteorological data	Meteorological data of historical periods.	China Meteorological Data Service Center (http://data.cma.cn/).
	Meteorological data in the future period (CMIP6).	Global Climate Research Program Center. (https://aims2.llnl.gov/search/cmip6/).
Soil data	Soil texture.	Resource and Environmental Science Data Platform (http://www.resdc.cn/).
	Other physical parameters include soil bulk density, saturated water conductivity, and residual water content.	Data Center of the Qinghai-Tibet Plateau in China (https://data.tpdc.ac.cn/home/).
	Soil moisture at different depths.	Google Earth Engine platform (https://code.earthengine.google.com/).
Winter wheat field trial dataset from the experimental station	Experimental data on winter wheat from agrometeorological stations, including the phenological period data of winter wheat from 1992 to 2013 and the yield data from 2000 to 2013.	China Meteorological Data Service Center (http://data.cma.cn/).

We conducted the DSSAT-CERES-Wheat model by improving the method of water stress factors (*SWFAC*). Under full irrigation conditions, potential root water uptake (*TRWUP*) is typically greater than potential root transpiration (EP_0). As root water absorption increases and surface evaporation rises, soil water content decreases, reducing *TRWUP*. This triggers the first drought stress factor (*TURFAC*) when a threshold is reached during a particular growth stage. When EP_0 equals or exceeds potential root water uptake, a second stress factor (*SWFAC*) emerges, which predominantly affects processes related to crop growth and biomass formation (He et al., 2013). The improved nonlinear SWFAC (Fig. 2) was used to quantify the effect of drought stress on winter wheat yield (Yao et al., 2025).

The genetic parameters in the DSSAT model are related to crop growth, development, and yield accumulation, and only when appropriate genetic parameters are found can the phenological period and yield prediction be more accurate (Wei et al., 2022; Yao et al., 2022). The DSSAT-CERES-Wheat model has three related to phenological periods and four related to growth (Table 2). Crop model output variables of winter wheat phenology (flowering and maturity), maximum leaf area index, evapotranspiration, above-ground biomass, grain yield, and field observations were used to estimate parameters and validate the model. The winter wheat data from 1981 to 2021 were divided randomly into two datasets at a 7:3 ratio, with 70 % of the data for model calibration and 30 % for model validation. The default values required for program operation are set during parameter estimation. The generalized likelihood uncertainty estimation (GLUE) approach was used to estimate the genetic coefficients (He et al., 2010).

In this study, the modular mean absolute error (*RMAE*) and the relative root mean square error (*RRMSE*), which can measure the relative difference between simulated and measured values, can be compared between different variables (He et al., 2010; Yao et al., 2020).

The specific calculation formula of *RMAE* is as follows:

$$RMAE = \frac{1}{n}\sum_{i=1}^{n}\frac{|S_i - O_i|}{|O_i|} \times 100\% \quad (1)$$

The specific calculation formula of RRMSE is as follows:

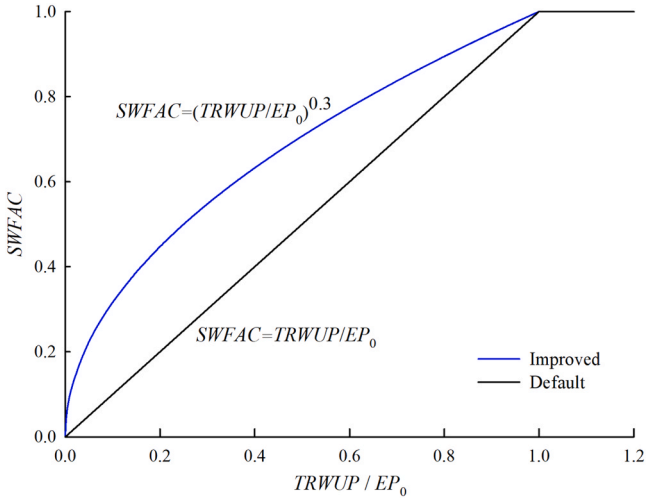

Fig. 2. Default and a modified water stress response functions for water stress factors (*SWFAC*). The *TRWUP was* potential root water uptake, EP_0 *was* potential root transpiration. The black line represents the default *SWFAC*; the blue line represents the improved nonlinear *SWFAC*.

Table 2
Genetic coefficients for the DSSAT-CERES-Wheat model.

Parameters	Parameters definition	Parameters range	Unit
P1V	Vernalization sensitivity coefficient stage at the optimum temperature	5–65	d
P1D	Photoperiod sensitivity coefficient	0–95	%
P5	Thermal time from the onset of linear fill to maturity	300–800	℃ d
G1	Kernel number per unit stem + spike weight at anthesis	15–30	No g^{-1}
G2	Potential kernel growth rate	20–65	mg
G3	Tiller death coefficient. Standard stem + spike weight when elongation ceases	1–2	g
PHINT	Thermal time between the appearance of leaf tips	60–100	℃ d

$$RMSE = \sqrt{\frac{1}{n}\sum_{i=1}^{n}(S_i - O_i)^2} \quad (2)$$

$$RRMSE = \frac{RMSE}{\overline{O}} \times 100\% \quad (3)$$

where S_i represents the i th simulated value, $\overline{S}$representing the average value of S_i; O_i represents the i th observed value, $\overline{O}$representing the average value of O_i; n is the number of samples. In general, the smaller the *RMAE* and *RRMSE* values, the higher the simulation accuracy of the model.

2.2.2. Statistical downscaling

Using the NWAI-WG statistical downscaling method, monthly data from 27 GCM models under various climate scenarios in CMIP6 were downscaled both temporally and spatially to enhance the spatio-temporal resolution of the GCM data (Liu, Zuo, 2012). This approach provided daily meteorological data for 77 meteorological stations across the Middle and upper reaches of Yellow River basin from 1961 to 2100. The effectiveness of this method has been validated and applied in previous studies (Feng et al., 2019).

(1) Downscaling the GCM data space

The inverse distance weighted (IDW) interpolation method interpolates the monthly GCM data. This method can eliminate the compensation effect between the grids and make the daily time scale data of GCM after spatial downscaling more accurate and the spatial distribution smoother. The calculation formula is as follows:

$$SD_i = \sum_{k=1}^{4}\left[\frac{1}{d_{i,k}^3}\left(\sum_{j=1}^{4}\frac{1}{d_{i,j}^3}\right)^{-1} p_k\right] \quad (4)$$

where SD_i is the GCM value after downscaling the i site; $d_{i,k}$ is the distance between the i th site and the surrounding k th cell (k = 1, 2, 3, 4); p_k is the GCM value of the k th cell.

(2) Deviation correction of GCM data

The deviation between the measured values of P, T_{max}, and T_{min} and the downscaling values of GCM space from 1961 to 2000 was corrected by drawing a Q-Q graph, and the deviation correction function of P, T_{max}, and T_{min} at each station was obtained. It is assumed that the change of the downscaling meteorological elements data of each GCMs space follows the deviation correction function and is linearly correlated with the observed values. The corrected GCMs values are calculated using the linear interpolation method, and the obtained parameters are applied to future scenario models (Chen, 2021).

(3) Time scaling of GCM data after spatial scaling

The weather generator (WGEN) is vital for studying climate change impacts and can simulate day-to-day meteorological information. A modified random weather generator was employed to downscale the monthly GCM data from the Middle and upper reaches of Yellow River basin meteorological stations to a daily time scale.

(4) Statistical downscaling effect evaluation

Taylor's diagram and the skill score (S) were used to evaluate the effectiveness of the NWAI-WG statistical downscaling method for each climate model. This evaluation approach comprehensively considers various meteorological elements' standard deviation and correlation coefficient, providing a holistic assessment of the downscaling performance. The calculation method for the skill score is represented by the following formula (Taylor, 2001):

$$S = \frac{4(l+R)^2}{\left(\frac{\sigma_f}{\sigma_r} + \frac{\sigma_r}{\sigma_f}\right)^2 (1+R_0)^2} \quad (5)$$

where R is the correlation coefficient; R_0 is the maximum value of the correlation coefficient. σ_f and σ_r are the standard deviations of the time series of simulated and observed meteorological elements, respectively. S is for Taylor skills. The larger the S value, the better the simulation effect of GCM mode.

Interannual Variation skill Score (*IVS*) was used to evaluate the time-scaling accuracy of the NWAI-WG downscaling method for 27 GCM. *IVS* calculation formula is shown in formula (6):

$$IVS = \left(\frac{STD_m}{STD_o} - \frac{STD_o}{STD_m}\right)^2 \quad (6)$$

where STD_m and STD_o are the inter-annual standard deviations of the time series of simulated and observed meteorological elements, respectively. The smaller the *IVS* value, the better the simulation effect of GCM mode.

2.2.3. Assessing wheat yield reduction and water productivity

Based on the measured data of winter wheat phenology and yield in the Middle and upper reaches of Yellow River basin in the historical period, the phenology and yield of winter wheat in the future were predicted by the DSSAT model. Specific methods and steps: The improved DSSA-CERES-Wheat model was verified according to the measured data in the historical period, and the changes in flowering, maturity, and yield of winter Wheat in different regions of the Middle and upper reaches of Yellow River basin were predicted under different scenarios (SSP2–4.5 and SSP5–8.5) in the future period (2022–2050). By comparing the relationship between winter wheat phenology and yield across different scenarios and regions, the study aimed to uncover the growth and development patterns of winter wheat in the Middle and upper reaches of Yellow River basin during the future period and assess changes in yield from the past to the future.

The rate of increase can be used to observe changes in yield intuitively, and the calculation method is presented in formula (7):

$$Z = \left(Y_j - Y_i\right)/Y_i \times 100\% \quad (7)$$

where Z is the yield increase rate (%); Y_j is the optimal planting date or winter wheat yield under the optimal planting date and optimal irrigation scenario in the future period (kg/ha); Y_i is the historical winter wheat yield (kg/ha).

Based on water productivity (WPc), the efficiency of dry matter production per unit of water consumed (i.e., evapotranspiration) was analyzed for different regions within the middle and upper reaches of the Yellow River Basin under various future scenarios. The specific calculation method is presented as follows (Kijne et al., 2003):

$$WPc = Y/ET \quad (8)$$

where *WPc* is water productivity, *Y* is winter wheat yield (kg/ha), *ET* is the total water consumption during the growth and development of winter wheat, calculated according to the water balance (mm).

2.2.4. Strategies for winter wheat production to cope with drought

Based on the precipitation data from 2020 to 2050 under various CMIP6 scenarios, the Pearson Type III frequency curve was used to identify typical hydrological years for each region in the Middle and upper reaches of Yellow River basin. The years corresponding to the 25 %, 50 %, and 75 % precipitation frequencies for all regional stations were classified as wet, normal, and dry years, respectively. The procedure was as follows: Precipitation data for the 31-year winter wheat growing period was first arranged in ascending order. The Pearson Type III curve was then applied to fit the precipitation series. By calculating the cumulative probabilities associated with different precipitation levels, the years corresponding to 50 % and 75 % cumulative probabilities were identified to determine normal and dry years for the future period. This study used the Hohai University version of hydrologic Pearson Type III curve parameter calculation and plotting software to calculate the frequencies associated with different precipitation levels. Additionally, the Wuhan University version of hydrologic frequency distribution curve fitting software was utilized to draw the hydrologic frequency curves.

Sowing date and irrigation are critical factors influencing the growth and yield of winter wheat. Identifying the optimal sowing time and irrigation practices is essential for efficient production. To address drought and enhance yields, determining the optimal planting dates under future climate change scenarios and identifying the best irrigation strategies for regions based on predicted wet, normal, and dry years are crucial.

Winter wheat is typically sown between September and October. Based on historical average sowing dates, planting was scheduled every five days, including the historical average, five days earlier and later, ten days earlier and later, and fifteen days earlier and later, resulting in seven planting dates. The improved DSSAT-CERES-Wheat model was employed to simulate winter wheat phenology and yield across these different sowing dates. By comparing phenological changes, the planting date with the highest yield was selected for each region.

Irrigation was necessary during both normal and dry years across the three regions delineated using the Pearson Type III distribution. To optimize irrigation strategies, we accounted for regional water availability and irrigation quotas for winter wheat under both climatic conditions. Key factors such as soil moisture and effective root zone depth were also considered. Notably, over 95 % of the winter wheat root system is confined to the 0–100 cm soil layer. In the middle and upper reaches of the Yellow River Basin, soil moisture within this layer typically ranges from 130 to 160 mm in normal years and decreases to 100–130 mm during drought years. Among the three regions, Region 1 exhibited the lowest soil moisture levels, indicating comparatively drier conditions.

We developed a range of irrigation scenarios based on the three key factors—local irrigation quotas, soil moisture levels, and the root depth of winter wheat. These scenarios aim to ensure that, after irrigation, soil moisture reaches 70–85 % of the field capacity. This range provides sufficient water to support the normal growth of winter wheat throughout its development stages and helps prevent yield reduction caused by insufficient soil moisture. In Region 1, the irrigation levels were set at 40 mm and 70 mm for normal years, and 60 mm and 90 mm for dry years. The various irrigation levels were, 40 mm and 60 mm in normal years, and 60 mm and 80 mm in dry years for Regions 2 and 3. Additionally, irrigation periods were set during the overwintering, jointing, and filling stages. Using the border irrigation method, fourteen scenarios were developed for normal and dry years (Table S2 and Table S3).

2.2.5. Uncertainty analysis

In this study, the combined meteorological data of GCMs and SSPs were used to predict the uncertainty of winter wheat yield in the future period, and the contribution of SSPs, GCMs, and their interaction to the yield was considered by analysis of variance (ANOVA) to analyze the uncertainty of the yield forecast from 2022 to 2050. The specific calculation process is as follows:

$$SST = SS_{SSPs} + SS_{GCMs} + SS_{GCMs:SSPs} \quad (9)$$

where *SST* is the total sum of squares, SS_{SSPs}, SS_{GCMs}, and $SS_{GCMs:SSPs}$ are respectively SSPs, GCMs, and the squared variance under their interaction. In this study, the average value of the final simulation results of 27 GCM was used to reduce the impact of uncertainty on the results.

3. Results

3.1. Evaluation of future climate models

The precipitation, T_{max}, and T_{min} correlation coefficients exceed 0.95 (Fig. 3). The T_{max} shows slightly higher correlation coefficients, ranging from 0.97 to 0.98, while the correlation coefficients for precipitation and T_{min} range from 0.95 to 0.97. The *S* values range of T_{max} T_{min}, and *P* were from 0.96 to 0.97, 0.90–0.93, 0.92–0.94, respectively (Fig. 3 and Table S4). The *S* values were all greater than 0.90, which indicate that the NWAI-WG statistical downscaling method can effectively perform spatial scaling for T_{max}, T_{min}, and *P* while meeting accuracy requirements for future projections.

3.2. Model parameter adjustment

With the GLUE-estimated genetic coefficients (Table S5), the simulated values of the improved DSSA-CERES-Wheat model for flowering and maturation of winter Wheat were consistent with the measured values. The *RMAE* and *RRMSE* were less than 7.82 %, and most were less than 5.00 % (Fig. 4 and Table S6). The *RMAE* and *RRMSE* for the DSSAT-CERES-Wheat model's simulation calibration and validation of winter wheat yield were reliable, with both metrics remaining below 19.00 %.

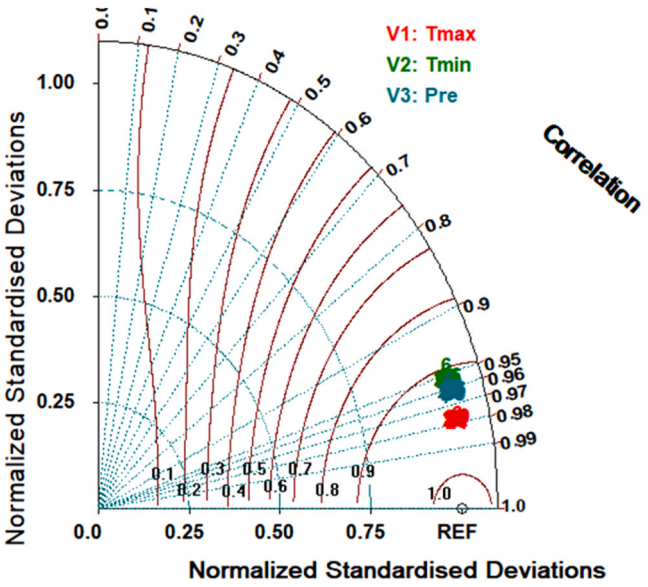

Fig. 3. Taylor plot comparing simulated and observed climate indices from 27 climate models at winter wheat stations in the middle and upper reaches of the Yellow River basin. The dotted green radial line represents the correlation coefficient (*r*) between simulated and observed values for different GCM models. The green arc shows the standard deviation of the GCM patterns, while the brown arc indicates the skill score (*S*) for the 27 GCM models.

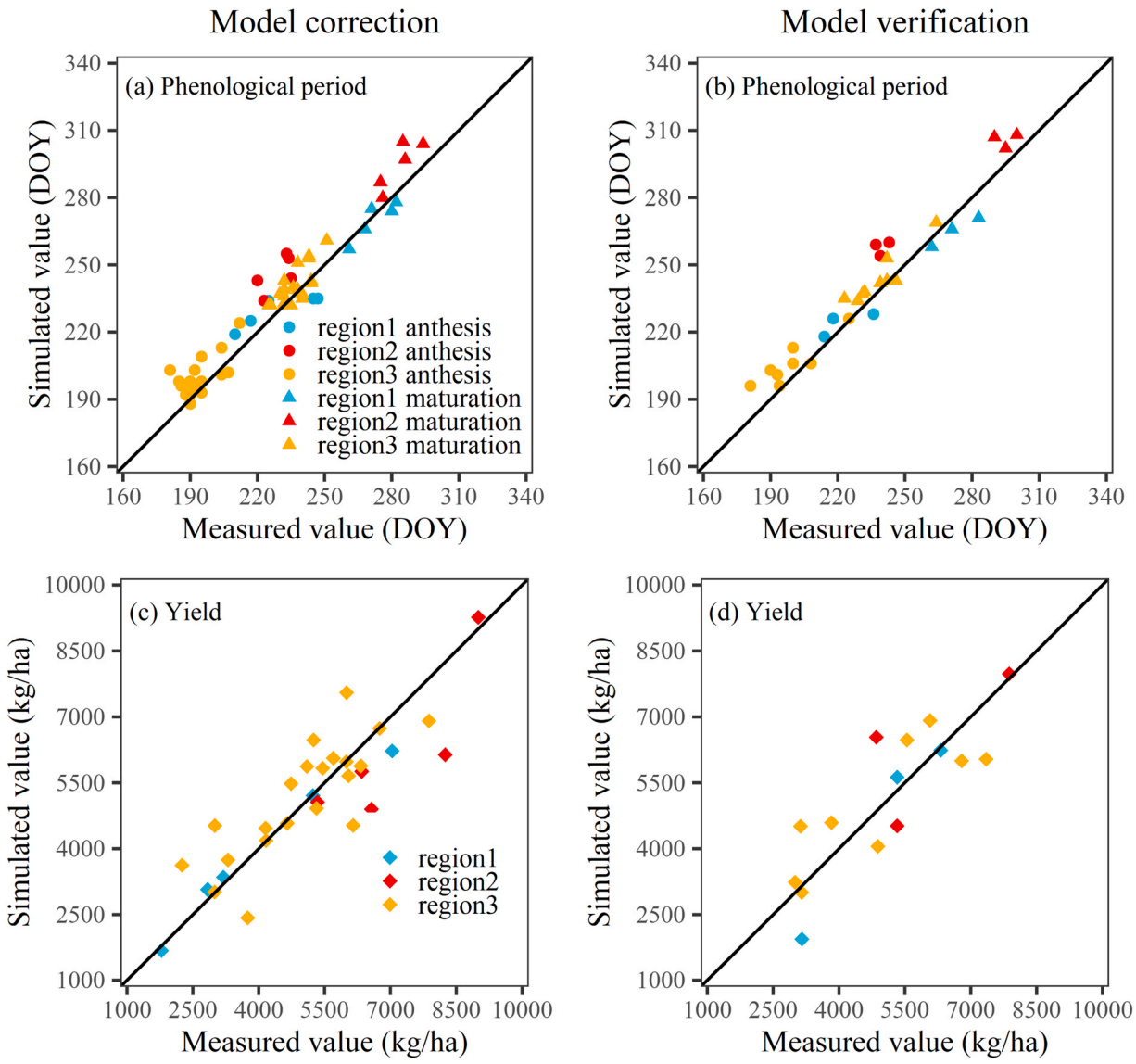

Fig. 4. Correction and verification of winter Wheat phenology and yield by improved DSSA-CERES-Wheat model.

It could be seen that the simulation effect of the anthesis period and maturity stage was slightly better than that of yield. The improved DSSAT-CERES-Wheat model has a better simulation effect on the phenological period of regions 1 and 3 than that of region 2, and has the best simulation effect on the yield of region 1, which is close to that of region 2 and region 3. In general, the improved DSSAT-CERES-Wheat model can simulate the growth and development of winter wheat in the three regions of the Middle and upper reaches of Yellow River basin, and the simulation results are similar. However, the simulation results of region 1 are the best, showing that the improved DSSAT-CERES-Wheat model can simulate the phenological period and yield of winter wheat.

3.3. Simulation of the growth and development in the future period

3.3.1. Effects of different sowing dates on winter wheat growth and yield

Under the influence of climate change, adjusting the sowing date can significantly impact winter wheat's growth, development, and yield. Region 2 has the latest anthesis period with the smallest standard deviation, indicating that the improved DSSAT-CERES-Wheat model produced more consistent anthesis period simulations for this region (Fig. 5). In contrast, Region 3 has the earliest anthesis period and the largest standard deviation, suggesting greater variability in anthesis timing. As the sowing date is advanced or delayed (from the first to the last row), the anthesis period changes more significantly than the normal sowing date. In region 1, the simulated anthesis period for different planting dates ranges between 220 and 235 days after sowing, while in Region 2, it spans 230–245 days. Region 3 shows a range of about 200–215 days, with an adjustment range of 30 days, indicating that flowering date changes less dramatically than sowing date changes. Under the SSP5–8.5 scenario, the anthesis period occurs slightly earlier compared to SSP2–4.5, suggesting that earlier sowing delays flowering while delayed sowing advances it. Based on historical average planting dates, the simulated anthesis period across all three regions is shorter than the historical average anthesis period. The variation in the anthesis period is small and similar in Regions 1 and 3, while region 2 shows greater variability. The figure also indicates that the winter wheat anthesis period tends to advance from 2022–2030, 2031–2040 and further to 2041–2050, suggesting a gradual advancement of flowering under climate change. The changes in winter wheat's maturity period are consistent with those observed in the anthesis period (Fig. S1).

Under the SSP2–4.5 and SSP5–8.5 scenarios from 2022 to 2050, the improved DSSAT-CERES-Wheat model simulated winter wheat yields for seven different planting dates (Fig. 6). Region 2 exhibited the highest yield, while Region 1 had the lowest, with Region 3 slightly

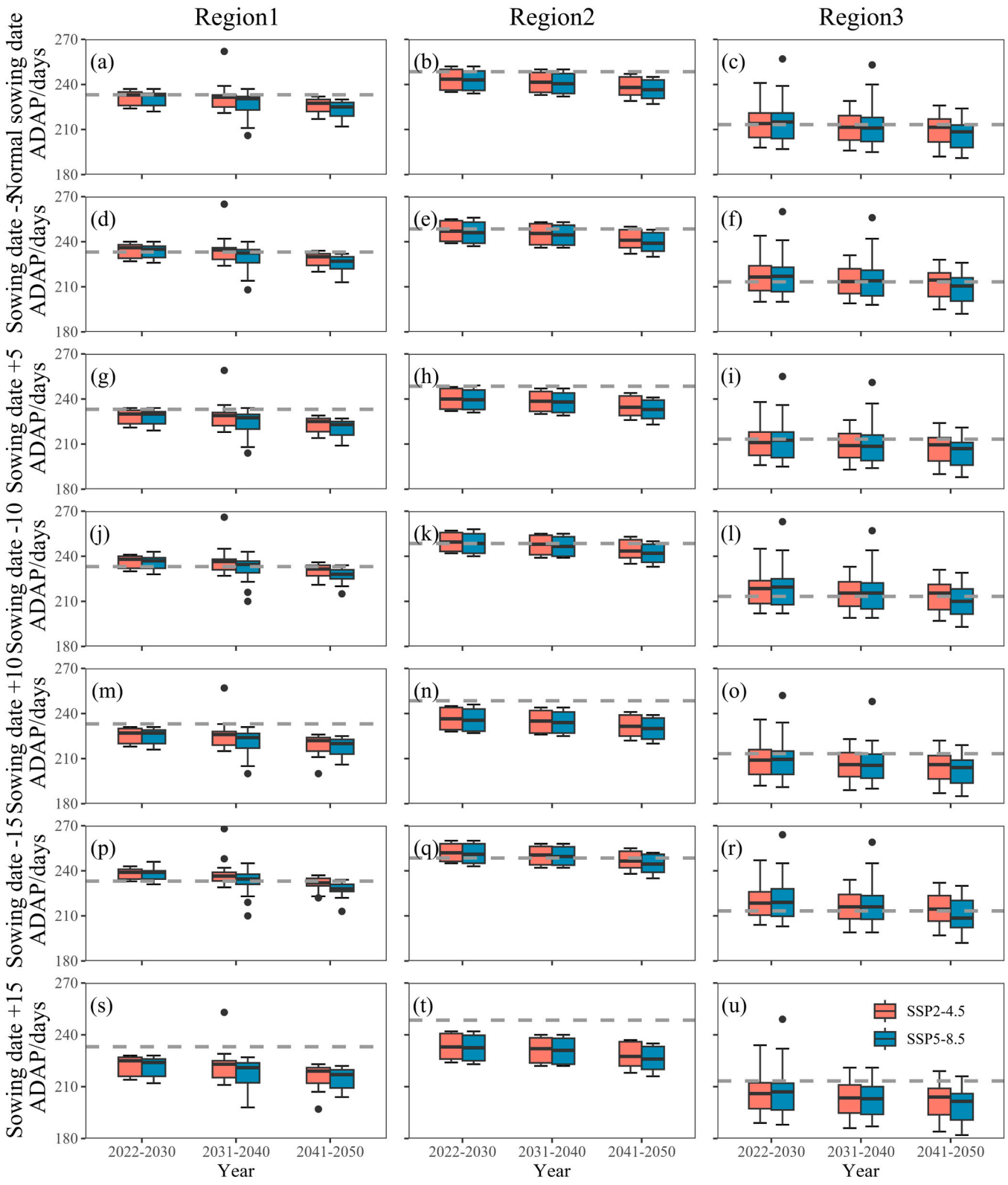

Fig. 5. The box plot of the winter Wheat anthesis period (ADAP) was simulated by DSAT-CERES-Wheat model with different seeding dates under SSP2–4.5 and SSP5–8.5 scenarios in the future period. Each column represents the three different regions, and each row corresponds to a different sowing date. The gray dashed line indicates the historical average anthesis period, the red box represents growth and development results under SSP2–4.5, the blue box under SSP5–8.5, with the black horizontal line inside the box representing the mean, error bars showing the standard deviation, and black dots indicating outliers. The same as below.

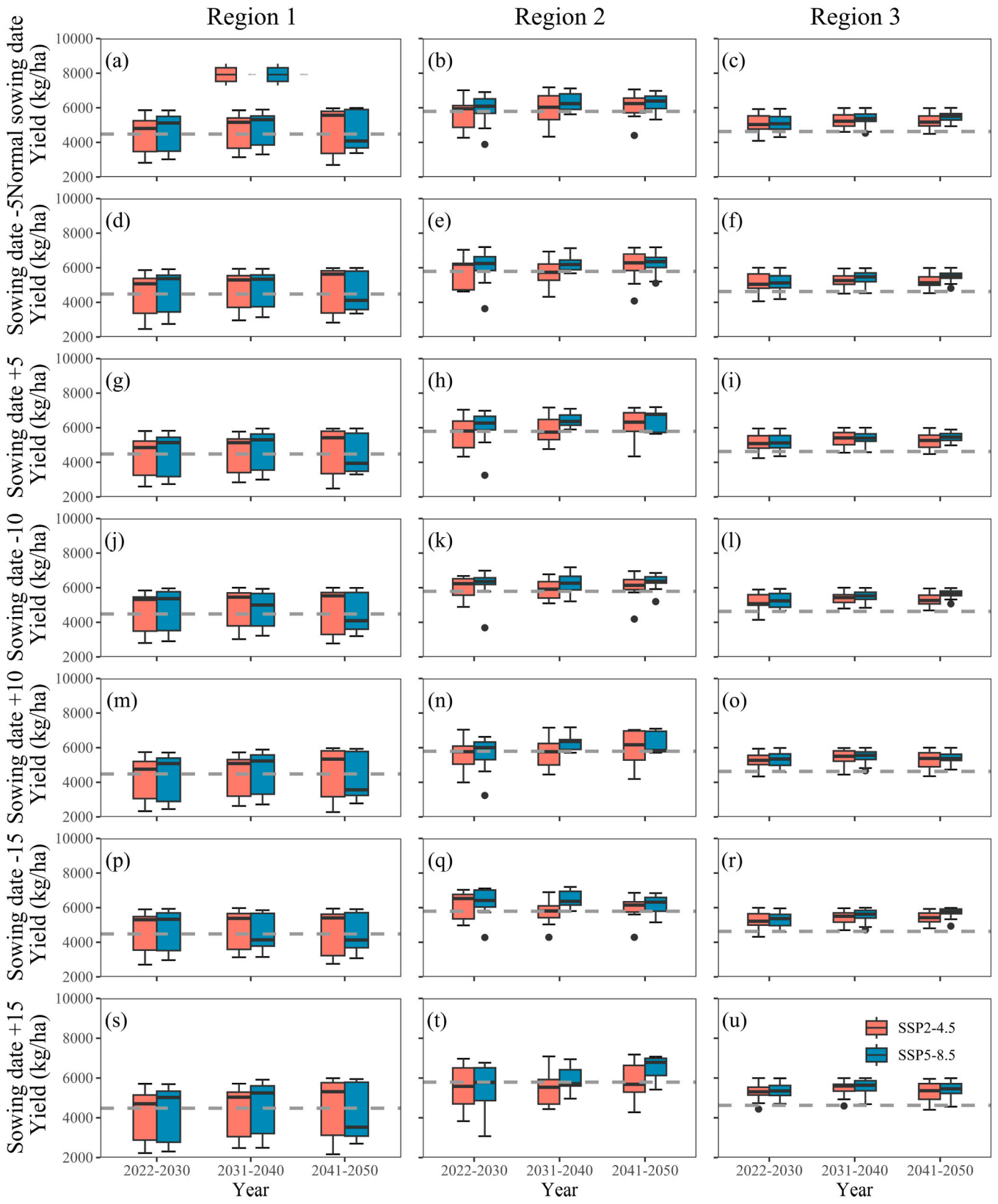

Fig. 6. The box plot of winter Wheat yield (HWAM) was simulated by improved DSAT-CERES-Wheat model with different sowing dates under SSP2–4.5 and SSP5–8.5 scenarios in the future period.

outperforming region 1. However, the box plot for region 3 was smaller, and the error bars were shorter than those for regions 1 and 2, indicating that the model produced more consistent yield simulations with less variability for region 3. Based on the historical average planting date, the simulated average yield for all three regions was higher than the historical average yield. Regions 1 and 3 yielded significant variability, while the yield in region 2 remained relatively stable. As shown in Fig. 6, yields varied significantly with the number of days the planting date was advanced or delayed. Under the SSP2–4.5 scenario, the average yield across the three regions was generally lower than under the SSP5–8.5 scenario. However, the average yield for region 1 under SSP2–4.5 was higher than under SSP5–8.5 from 2041 to 2050. Overall, winter wheat production is expected to increase from 2022 to 2050. The optimal planting dates of different regions under SSP2–4.5 and SSP5–8.5 scenarios in the future period are shown in Table 3. Based on the optimal sowing date and the actual production situation, we set a 7-day sowing window 3 days before and 3 days after the optimal sowing date, which can be adjusted according to the actual situation.

The change rates of winter wheat anthesis and mature period under different scenarios in the future period under the background of climate change compared with the historical period, blue represents advance, and red represents delay (Fig. 7). The changing rates of anthesis period and maturity stage were between −7.8 %-4.1 % and −8.1 %-2.8 %, respectively. The advance trend was larger than delay, and the maturity stage was more advanced than the anthesis period. Region 1 and region 2 were mostly advanced, and the trend of anthesis and mature period under SSP5–8.5 was more evident than that under SSP2–4.5. Region 3 shows a delay, and the change trend is more evident in the SSP5–8.5 scenario than in SSP2–4.5. With time, the absolute change rates of flowering and maturity in region 1 and region 2 increased, especially the change rate of region 2 was about −6 % from 2040 to 2050 under the SSP5–8.5 scenario. The change rates of flowering and maturation in region 3 gradually decreased with time, and the change rates of phenology from 2022 to 2032 were the largest, especially under the SSP5–8.5 scenario, where the change rates of flowering and maturation reached 4.1 % and 2.8 %, respectively. Region 1 shows an earlier trend, but the blooming and ripening period in 2035 is delayed under SSP5–8.5 scenario, and the number of days advanced in 2042 and 2044 under SSP2–4.5 scenario is the highest. Overall, the change rate of the winter wheat anthesis period in the future was greater than that of the maturity stage.

The changes in water stress factors affect winter wheat under the SSP2–4.5 and SSP5–8.5 scenarios in the future within the context of climate change (Fig. 8). The three columns at the top and Middle of the figure represent the average values of these water stress factors during the historical period. The circle's left and right sides in the figure correspond to winter wheat's water stress factors in three different regions under the SSP5–8.5 and SSP2–4.5 scenarios, respectively. Region 2 experiences the highest water stress factor, reaching approximately 0.65. The water stress factors for regions 1 and 3 are similar, with Region 1 having slightly lower water stress than region 3 during the historical period, around 0.15 and 0.25, respectively. In the future period, which is contrary to the historical trend, at about 0.15 and 0.12, respectively. From the historical to future periods, the water stress factors in Regions 1 and 2 show little change, whereas the water stress factor in region 3 decreases significantly. Over the future period, the water stress factor is expected to decline gradually from 2022 to 2050.

Table 3
The optimal sowing date and sowing window of the maximum yield in different scenarios and regions in the future period.

Region	Scene	Optimal sowing date	Sowing date window
Region 1	SSP2–4.5	The sowing date is 10 days ahead of schedule	(−13 , −7)
	SSP5–8.5		(−13 , −7)
Region 2	SSP2–4.5	The sowing date is 15 days ahead of schedule	(−18 , −12)
	SSP5–8.5		(−18 , −12)
Region 3	SSP2–4.5	The sowing date is 15 days ahead of schedule	(−18 , −12)
	SSP5–8.5		(−18 , −12)

3.3.2. *Effects of different irrigation scenarios on the winter wheat growth and yield*

The rainfall corresponding to the average rainfall frequency of 50 % and 75 % in the region was found according to the Pearson III curve (Fig. S2). The years of normal water and dry years that need irrigation in different regions in the future were found according to the rainfall, and the specific years are shown in Table S7. Based on the optimal planting dates for different scenarios in the future, Fig. 9 illustrates changes in winter wheat yield under various irrigation scenarios in normal and dry years across different regions. Across different irrigation scenarios, yields in dry years were generally higher than in normal years. However, under the SSP2–4.5 scenario, region 1 showed higher yields during normal than dry years. The yield increase under the SSP2–4.5 scenario was greater than that under the SSP5–8.5 scenario, and winter wheat yields increased with higher irrigation amounts. In all three regions, the highest yields were achieved with irrigation during the overwintering, jointing, and filling periods, corresponding to the 14th irrigation scenario in each region in Table S2 and Table S3. Among all the irrigation scenarios (1, 2, 3, 8, 9, and 10) shown in the figure, scenarios 2 and 9 yielded the highest results, highlighting the jointing stage as a critical period for water demand in winter wheat cultivation in the Middle and upper reaches of Yellow River basin. Overall, irrigation during the overwintering, jointing, and filling stages positively influenced the growth and development of winter wheat.

The water productivity (WPc) of winter wheat is higher in region 2 than regions 1 and 3, with average values of approximately 1.50 in region 2, 1.20 in region 1, and 1.25 in region 3 (Fig. 10). Under the SSP2–4.5 scenario, the WPc during drought years in regions 2 and 3 exceeds that of normal years, while in region 1, the WPc is lower during drought years than in normal years. In contrast, under the SSP5–8.5 scenario, the WPc during drought years is higher than during normal years across all three regions. The WPc trends align with projected winter wheat yields, indicating that WPc increases as yields increase. Among the six irrigation scenarios evaluated (1, 2, 3, 8, 9, and 10), scenarios 2, 3, 9, and 10 showed the highest WPc. This finding highlights the importance of the jointing and filling stages for water demand in winter wheat growth within the Middle and upper reaches of Yellow River basin. For optimal irrigation, region 1 requires 70 mm and 90 mm of water during normal and dry years, respectively, while Regions 2 and 3 require 60 mm and 80 mm.

Winter wheat yield and yield growth in the Middle and upper reaches of Yellow River basin have been rising from the historical period to the future, with the optimal irrigation scenario showing a greater impact on yield increase than the optimal planting date (Table S8). In the future, the Middle and upper reaches of Yellow River basin's total yield increase rate under SSP2–4.5 scenario (20.62 %) is higher than that under SSP5–8.5 scenario (16.32 %). Under the SSP5–8.5 scenario, the yields were 18.82 %, 15.69 %, and 14.74 %, respectively. Under the SSP2–4.5 scenario, yields in regions 2 and 3 increased by over 21.00 %. In the Middle and upper reaches of Yellow River basin's future period, the yield increase rate based on the optimal planting date is lower under the SSP2–4.5 scenario than under the SSP5–8.5 scenario, at 5.96 % and 6.35 %, respectively. Conversely, the yield increase rate based on the optimal irrigation scenario is higher under the SSP2–4.5 scenario, at 14.12 % compared to 9.30 % under SSP5–8.5. In general, the total yield increase rate of winter wheat in the Middle and upper reaches of Yellow River basin is around 18.50 %, and the total yield increase rate under SSP2–4.5 scenario is slightly higher than that under SSP5–8.5 scenario, which is 20.62 % and 16.32 % respectively.

According to the above results, the sowing date of region 1 in the future period should be advanced by 10 days, the sowing window is (−13, −7), and the irrigation water should be 70 mm and 90 mm at the

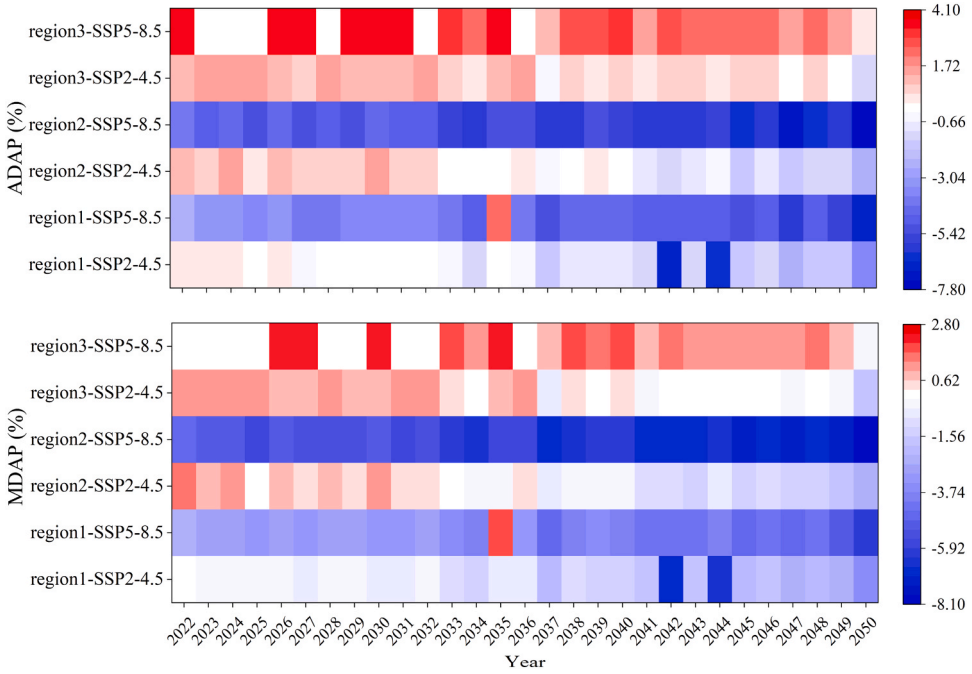

Fig. 7. Changes of the phenological period under SSP2–4.5 and SSP5–8.5 scenarios in the future period.

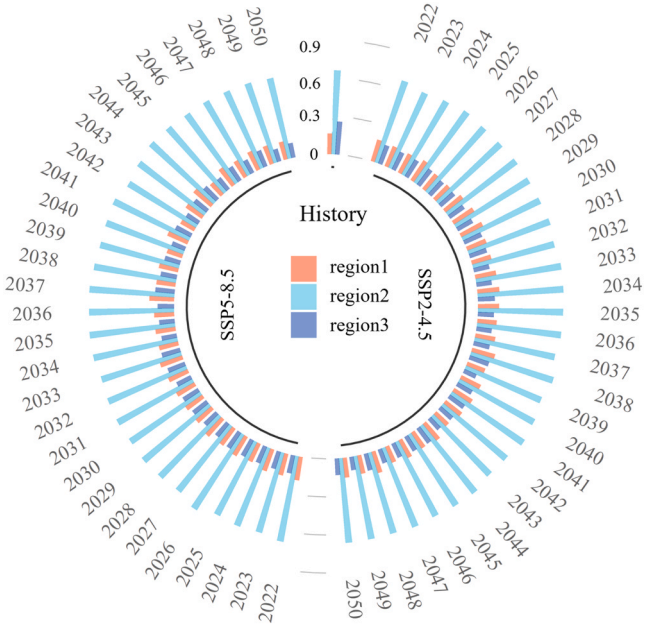

Fig. 8. Changes of stress factors under SSP2–4.5 and SSP5–8.5 scenarios in the future period.

jointing stage and filling stage in normal and dry years, respectively. In region 2, the sowing date should be advanced 15 days, the sowing window is (−18, −12), and the irrigation water should be 60 mm and 80 mm in jointing and filling periods in normal and dry years, respectively. In region 3, the sowing date should be advanced by 15 days, and the sowing window is (−18, −12). The irrigation water should be 60 mm and 80 mm in jointing and filling periods in normal and dry years, respectively, to avoid reducing winter wheat production under the background of drought in the future and achieve a high and stable yield of winter wheat.

4. Discussion

4.1. Influence of sowing date on winter wheat yield in future period

In the context of future climate change, extreme climate (such as drought, etc.) will lead to winter wheat yield reduction, an urgent problem to solve. We can prevent winter wheat yield reduction by adjusting the sowing date, so discussing the influence of sowing date change on winter wheat yield is significant. Qiao et al. (2023) modeled the optimal sowing date of global winter wheat based on optimality in simulated gross primary product. The results showed that mild warming promoted early sowing in humid regions but late sowing in arid regions, and severe warming led to delayed sowing in most regions. Wu et al. (2023) studied winter wheat in the Loess Plateau and showed that delayed seeding significantly extended the emergence time and decreased tillering number, leaf area index, root biomass, and above-ground biomass. The study of Sattar et al. (2023) on winter wheat in the Indo-Gangetic plain showed that the planting date significantly impacted the phenological duration, and the yield increased with the advance of the planting date. The results showed that early sowing of winter wheat in the Middle and upper reaches of Yellow River basin could improve the yield, and the best sowing date was 10 days earlier and, the sowing window was (−13, −7) in region 1, and the best sowing date was 15 days earlier and the sowing window was (−18, −12) in region 2 and 3. In addition, early sowing leads to the extension of flowering and maturity. In contrast, late sowing leads to the shortening of flowering and maturity, which may be because the growth and development of winter wheat need to go through the vernalization stage, which requires a particular low-temperature duration, about 0 ~ 5 degrees, and the low-temperature duration need to be greater than 35 days. Without the vernalization stage, it cannot enter the heading stage, and only vegetative growth can be carried out. Therefore, winter wheat sown early has a higher temperature at the beginning of growth and needs longer to reach the low temperature in the vernalization stage before heading. The vegetative growth time is longer, the accumulated nutrients are more, and the yield increases. Therefore, the flowering and maturity winter wheat sown early is extended, while the maturity period of winter wheat sown late is shortened.

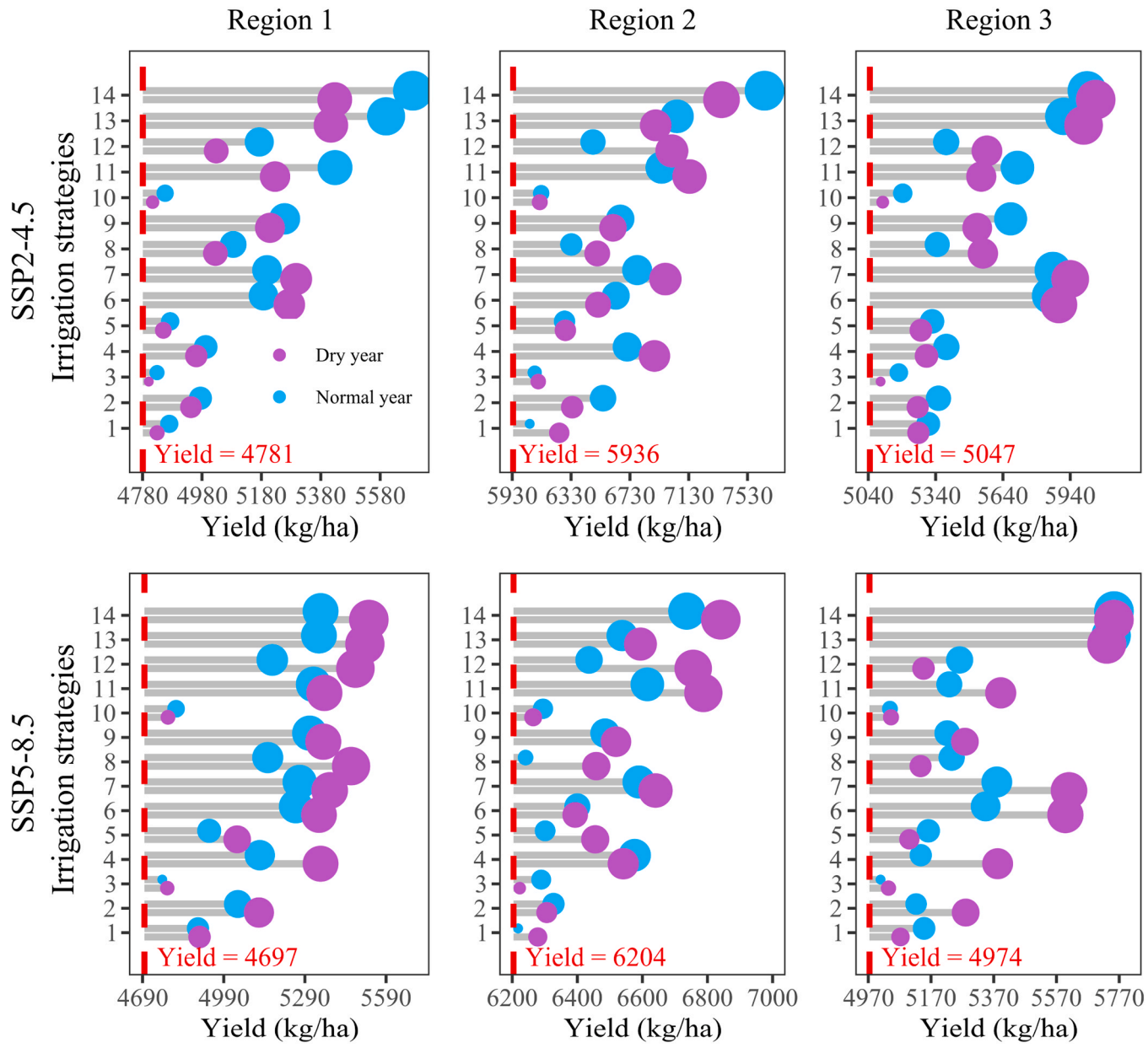

Fig. 9. Winter wheat yield under different irrigation strategies with optimal seeding date in future period. The red dotted line represents winter wheat yield under the optimal planting date. Blue dots indicate yields for normal years, while purple dots represent yields for dry years, with the size of the dots reflecting production levels. The vertical axis (1–14) corresponds to different irrigation treatments outlined (Table S2 and Table S3).

4.2. Effects of irrigation changes on winter wheat yield in future period

Besides the sowing date, irrigation strategies are critical in determining winter wheat yields. Studying winter wheat's key water demand periods and developing optimal irrigation strategies to support its growth and development is essential. Previous studies have identified the jointing stage as a crucial water demand period for winter wheat. Li et al. (2024) research on winter wheat in the North China Plain indicated that while future climate scenarios may slightly increase irrigation water requirements compared to historical periods, the water-sensitive periods (recovery, jointing, and anthesis) remain unchanged. Zhang et al. (2022) used the AquaCrop model to explore optimal irrigation methods for winter wheat in northwest China, finding that 90 mm of irrigation during the wintering period and varying amounts (0, 30, and 60 mm) during the jointing period were optimal for wet, normal, and dry years, respectively. Yang et al. (2018) found that soil volumetric water content at the jointing stage was related to efficient water-saving irrigation, indicating that the early jointing stage is optimal for irrigation. Further research on the winter wheat-summer corn rotation system in the North China Plain by Li et al. (2023) recommended 165 mm and 90 mm of irrigation during the jointing and anthesis stages, respectively. This study found that water productivity (WPc) was highest during the jointing and filling stages across the three regions of the Middle and upper reaches of Yellow River basin, suggesting that irrigation during these periods can help mitigate the impact of drought.

4.3. Uncertainty analysis of winter wheat yield

Forecasting winter wheat yields involves uncertainty due to the variability of future meteorological data and the inherent limitations of the DSSAT-CERES-Wheat model itself. Generally, using two SSP scenarios and 27 GCM models as inputs for crop models introduces certain uncertainties in predicting winter wheat yield (Wang et al., 2020; Jiang et al., 2022). Jiang et al. (2022) analyzed crop models, GCMs, SSPs, and

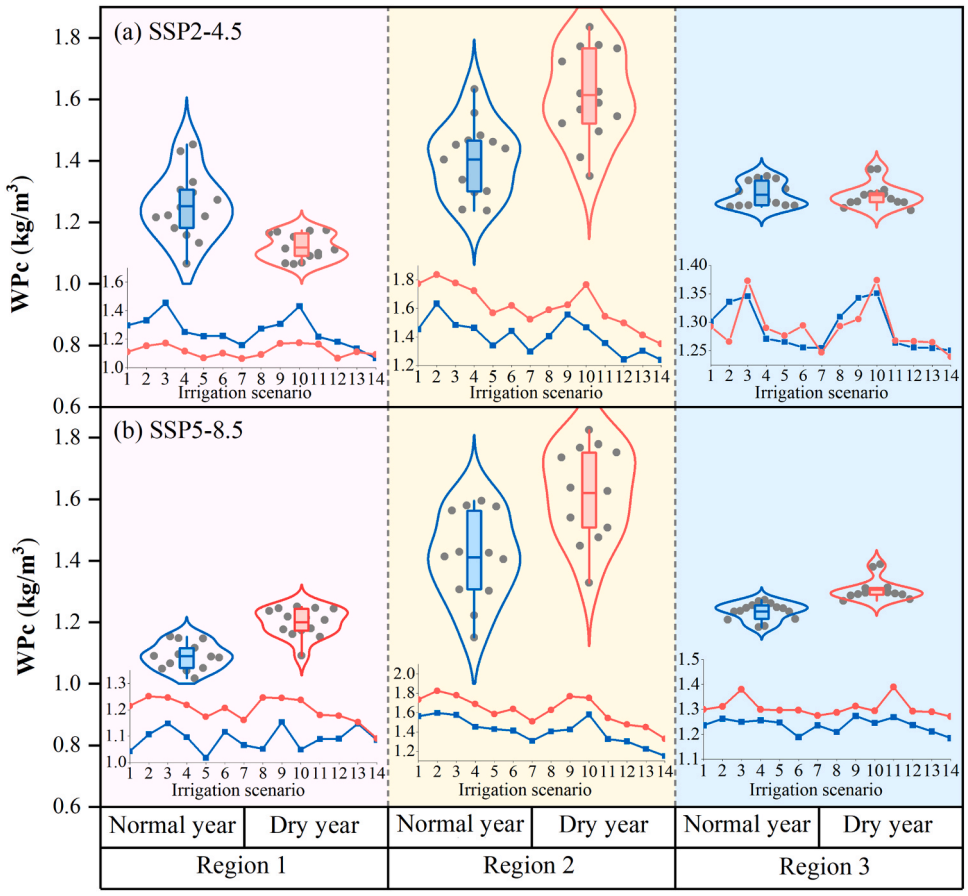

Fig. 10. Water productivity (WPc) in normal and dry years in different regions in the Future.

species distribution models (SDMs), finding that SDMs contributed most to uncertainty in winter wheat yield forecasts on the Loess Plateau. Wang et al., (2020b) showed that GCMs were the main source of uncertainty in wheat yield predictions in Australia, while crop models were the primary source in China, largely due to differing levels of uncertainty in GCM predictions of rainfall across regions. Additionally, input variables such as average temperature, precipitation, and solar radiation contribute to uncertainties in wheat yield predictions (Zare et al., 2022; Han et al., 2023). In this study, the uncertainty contributions of SSPs and GCMs were quantified using ANOVA. The analysis showed that uncertainty from GCMs in predicting winter wheat yield in the Middle and upper reaches of Yellow River basin from 2022 to 2050 was greater than that from SSPs or the interaction between SSPs and GCMs (Fig. S4). However, this study used only the improved DSSAT-CERES-Wheat model for yield predictions, which introduces its own set of uncertainties, potentially leading to errors in yield forecasting.

5. Conclusions

Winter wheat yields in the Middle and upper reaches of Yellow River basin are expected to increase with earlier sowing dates. Under the SSP2–4.5 and SSP5–8.5 scenarios, the optimal sowing time for Region 1 is 10 days earlier, with a sowing window of (−13, −7), leading to yield increases of 6.34 % and 4.47 %, respectively. For Regions 2 and 3, the optimal sowing time is 15 days earlier, with a sowing window of (−18, −12). Overall, the Middle and upper reaches of Yellow River basin yield is projected to increase by 5.96 % under the SSP2–4.5 scenario and by 6.35 % under the SSP5–8.5 scenario compared to historical levels.

The WPc is expected to increase along with winter wheat yield in the Middle and upper reaches of Yellow River basin in the future. The WPc ranks highest in region 2, followed by region 3, and lowest in region 1, mirroring the yield pattern across these regions. The optimal irrigation strategy for both normal and dry years involves irrigating during the jointing and filling stages, which are crucial for meeting the crop's water needs. Under SSP2–4.5 and SSP5–8.5 scenarios, the optimal combination of sowing date and irrigation for region 1 resulted in yield increases of 18.48 % and 18.82 %, respectively. The optimal sowing and irrigation for region 2 increased winter wheat yield by 21.55 % and 15.69 %, respectively.

The same irrigation strategy for region 3 increased yield by 21.52 % and 14.74 % under SSP2–4.5 and SSP5–8.5 scenarios, respectively. Across the Middle and upper reaches of Yellow River basin, the combination of optimal sowing dates and irrigation scenarios under SSP2–4.5 and SSP5–8.5 resulted in yield increases of 14.12 % and 9.30 %, respectively, compared to using optimal sowing dates alone. Compared to the historical period, these combined strategies resulted in yield increases of 20.62 % and 16.32 % under SSP2–4.5 and SSP5–8.5, respectively.

CRediT authorship contribution statement

Ning Yao: Writing – original draft, Formal analysis. **La Zhuo:** Resources, Funding acquisition. **Jiangfeng Xiangli:** Visualization, Supervision. **Li Linchao:** Validation, Resources. **Yingnan Wei:** Writing – original draft, Visualization. **Miaolei Hou:** Methodology, Data curation. **zhang ziya:** Visualization, Resources. **Jianqiang He:** Supervision, Methodology. **Tehseen Javed:** Writing – review & editing, Writing – original draft. **Qiang Yu:** Software, Resources.

Declaration of Competing Interest

The authors declare that they have no known competing financial

interests or personal relationships that could have appeared to influence the work reported in this paper.

Acknowledgments

This research was partially supported by the National Natural Science Foundations of China (52209070 and U2243235), the Shaanxi Provincial Water Conservancy Science and Technology Plan Project (2024slkj-10), and Cyrus Tang Foundation Project.

Appendix A. Supporting information

Supplementary data associated with this article can be found in the online version at doi:10.1016/j.agwat.2025.109678.

Data availability

Data will be made available on request.

References

Bai, H., Xiao, D., Tang, J., Liu, D., 2024. Evaluation of wheat yield in North China Plain under extreme climate by coupling crop model with machine learning. Comput. Electron. Agric. 217.

Chen X., 2021. Effects of meteorological and agricultural drought on growth and yield of winter wheat. Yang Ling: Northwest Agriculture and Forestry University. (In Chinese with English abstract).

Christian, J.I., Basara, J.B., Hunt, E.D., Otkin, J.A., Furtado, J.C., Mishra, V., Xiao, X., Randall, R.M., 2021. Global distribution, trends, and drivers of flash drought occurrence. Nat. Commun. 12 (1).

Feng, P., Liu, D., Wang, B., Waters, C., Zhang, M., Yu, Q., 2019. Projected changes in drought across the wheat belt of southeastern Australia using a downscaled climate ensemble. Int. J. Climatol. 39 (2), 1041–1053.

Gao, Z., Chen, X., Liu, X., 2007. Effects of soil water change on growth yield and water use efficiency of winter wheat. Trans. Chin. Soc. Agric. Eng. 23 (8), 52–58 (In Chinese with English abstract).

Han, W., Lin, X., Wang, D., 2023. Uncovering the primary drivers of regional variability in the impact of climate change on wheat yields in China. J. Clean. Prod. 421.

He, J., Cai, H., Bai, J., 2013. Irrigation scheduling based on CERES-Wheat model for spring wheat production in the Minqin Oasis in Northwest China. Agric. Water Manag. 128, 19–31.

He, J., Jones, J.W., Graham, W.D., Dukes, M.D., 2010. Influence of likelihood function choice for estimating crop model parameters using the generalized likelihood uncertainty estimation method. Agric. Syst. 103 (5), 256–264.

Hu, Q., Yang, N., Pan, F.F., Pan, X.B., Wang, X.X., Yang, P.Y., 2017. Adjusting sowing dates improved potato adaptation to climate change in Semiarid Region, China. Sustainability 9 (4).

Javed, T., Zhang, J., Bhattarai, N., Sha, Z., Rashid, S., Yun, B., Ahmad, S., Henchiri, M., Kamran, M., 2021. Drought characterization across agricultural regions of China using standardized precipitation and vegetation water supply indices. J. Clean. Prod. 313, 15.

Jia, Q., Jia, H., Li, Y., Yin, I., 2023. Applicability of CMIP5 and CMIP6 Models in China: reproducibility of Historical Simulation and Uncertainty of Future Projection. J. Clim. 36 (17), 5809–5824.

Jiang, T., Wang, B., Xu, X., Cao, Y., Liu, D., He, L., Jin, N., Ma, H., Chen, S., Zhao, K., Feng, H., Yu, Q., He, Y., He, J., 2022. Identifying sources of uncertainty in wheat production projections with consideration of crop climatic suitability under future climate. Agric. For. Meteorol. 319.

Jones, J.W., Hoogenboom, G., Porter, C.H., Boote, K.J., Batchelor, W.D., Hunt, L.A., Wilkens, P.W., Singh, U., Gijsman, A.J., Ritchie, J.T., 2003. The DSSAT cropping system model. Eur. J. Agron. 18 (3-4), 235–265.

Kijne, J.W., Barker, R., Molden, D., 2003. Water Productivity in Agriculture: Limits and Opportunities for Improvement (Comprehensive Assessment of Water Management in Agriculture Series 1). CABI, Wallingford.

Li, S., An, P., Pan, Z., Wang, F., Li, X., Liu, Y., 2015. Farmers' initiative on adaptation to climate change in the Northern Agro-pastoral Ecotone. Int. J. Disaster Risk Reduct. 12, 278–284.

Li, Y., Chang, J., Fan, J., Yu, B., 2021. Spatial-temporal evolution and driving mechanism of agricultural drought in the Yellow River Basin under climate and land use change. Chin. J. Agric. Eng. 37 (19), 84–93 (In Chinese with English abstract).

Li, H., Li, X., Mei, X., Nangia, V., Guo, R., Hao, W., Wang, J., 2023. An alternative water-fertilizer-saving management practice for wheat-maize cropping system in the North China Plain: Based on a 4-year field study. Agric. Water Manag. 276.

Li, M., Zhou, S., Shen, S., Wang, J., Yang, Y., Wu, Y., Chen, F., Lei, Y., 2024. Climate-smart irrigation strategy can mitigate agricultural water consumption while ensuring food security under a changing climate. Agric. Water Manag. 292.

Liu, X., Cao, K., Li, M., 2024. Assessing the impact of meteorological and agricultural drought on maize yields to optimize irrigation in Heilongjiang Province, China. J. Clean. Prod. 434.

Liu, D.L., Zuo, H., 2012. Statistical downscaling of daily climate variables for climate change impact assessment over New South Wales, Australia. Clim. Change 115 (3), 629–666.

Long, X., Ju, H., Wang, J., Gong, S., Li, G., 2022. Impact of climate change on wheat yield and quality in the Yellow River Basin under RCP8.5 during 2020-2050. Adv. Clim. Change Res. 13 (3), 397–407.

Ma, D., Bai, Z., Xu, Y., Gu, H., Gao, C., 2024. Assessing streamflow and sediment responses to future climate change over the Upper Mekong River Basin: A comparison between CMIP5 and CMIP6 models. J. Hydrol. Reg. Stud. 52.

Mu, L., Su, K., Zhou, T., Yang, H., 2023. Yield performance, land and water use, economic profit of irrigated spring wheat/alfalfa intercropping in the inland arid area of northwestern China. Field Crops Res. 303.

Qiao, S., Harrison, S.P., Prentice, I.C., Wang, H., 2023. Optimality-based modelling of wheat sowing dates globally. Agric. Syst. 206.

Quandt, A., 2021. Coping with drought: narratives from smallholder farmers in semi-arid Kenya. Int. J. Disaster Risk Reduct. 57.

Rahimi-Moghaddam, S., Deihimfard, R., Azizi, K., Roostaei, M., 2021. Characterizing spatial and temporal trends in drought patterns of rainfed wheat (Triticum aestivum L.) across various climatic conditions: a modelling approach. Eur. J. Agron. 129, 16.

Sattar, A., Nanda, G., Singh, G., Jha, R.K., Bal, S.K., 2023. Responses of phenology, yield attributes, and yield of wheat varieties under different sowing times in Indo-Gangetic Plains. Front. Plant Sci. 14.

Shi, X., Chen, J., Ding, H., Yang, Y., Zhang, Y., 2024. Winter wheat yield estimation based on sparrow search algorithm combined with random forest: a case study in Henan Province, China. Chin. Geogr. Sci. 34 (2), 342–356.

Shiferaw, B., Smale, M., Braun, H.J., Duveiller, E., Reynolds, M., Muricho, G., 2013. Crops that feed the world 10. Past successes and future challenges to the role played by wheat in global food security. Food Secur 5291–5317.

Sun, S., Yang, X., Zhang, Z., Zhao, J., Liu, Z., 2021. Effects of different levels of drought on winter wheat yield in North China Plain. Chin. J. Agric. Eng. 37 (14), 69–78 (In Chinese with English abstract).

Taylor, K.E., 2001. Summarizing multiple aspects of model performance in a single diagram. J. Geophys. Res. Atmos. 106 (D7), 7183–7192.

Tu, D., Jiang, Y., Zhang, L., Cai, M., Li, C., Cao, C., 2022. Effect of various combinations of temperature during different phenological periods on indica rice yield and quality in the Yangtze River Basin in China. J. Integr. Agric. 21 (10), 2900–2909.

Wang, B., Feng, P., Liu, D., O'Leary, G.J., Macadam, I., Waters, C., Asseng, S., Cowie, A., Jiang, T., Xiao, D., Ruan, H., He, J., Yu, Q., 2020a. Sources of uncertainty for wheat yield projections under future climate are site-specific. Nat. Food 1 (11), 720.

Wang, X., Yang, D., Feng, X., Cheng, C., Zhou, C., Zhang, X., Ao, Y., 2020b. Impact of ecological restoration on water resources in the middle Yellow River Basin. Bull. Soil Water Conserv. 40 (06), 205–212 (In Chinese with English abstract).

Wei, Y., Ru, H., Leng, X., He, Z., Ayantobo, O.O., Javed, T., Yao, N., 2022. Better performance of the modified CERES-wheat model in simulating evapotranspiration and wheat growth under water stress conditions. Agriculture 12 (11), 15 (In Chinese with English abstract).

Wu, J., Cheng, G., Wang, N., Shen, H., Ma, X., 2022. Spatiotemporal patterns of multiscale drought and its impact on winter wheat yield over North China Plain. Agronomy 12 (5).

Wu, L., Quan, H., Wu, L., Zhang, X., Feng, H., Ding, D., Siddique, K.H.M., 2023. Responses of winter wheat yield and water productivity to sowing time and plastic mulching in the Loess Plateau. Agric. Water Manag. 289.

Yang, C., Fraga, H., van Ieperen, W., Trindade, H., Santos, J.A., 2019. Effects of climate change and adaptation options on winter wheat yield under rainfed Mediterranean conditions in southern Portugal. Clim. Change 154 (1-2), 159–178.

Yang, Y., Huang, Y., Zhang, Y., Tong, X., 2018. Optimal irrigation mode and spatio-temporal variability characteristics of soil moisture content in different growth stages of winter wheat. Water 10 (9).

Yao, N., Li, Y., Liu, Q., Zhang, S., Chen, X., Ji, Y., Liu, F., Pulatov, A., Feng, P., 2022. Response of wheat and maize growth-yields to meteorological and agricultural droughts based on standardized precipitation evapotranspiration indexes and soil moisture deficit indexes. Agric. Water Manag. 266.

Yao, N., Li, Y., Xu, F., Liu, J., Chen, S., Ma, H.J., Chau, H.W., Liu, D., Li, M., Feng, H., Yu, Q., He, J., 2020. Permanent wilting point plays an important role in simulating winter wheat growth under water deficit conditions. Agric. Water Manag. 229, 15.

Yao, N., Wei, Y.N., Jiang, K.H., Liu, J., Li, Y., Ran, H., Javed, T., Feng, H., Yu, Q., He, J. Q., 2025. Nonlinear water stress response functions can improve the performance of the DSSAT-CERES-Wheat model under water deficit conditions. Agric. Water Manag. 307.

Zare, H., Weber, T.K.D., Ingwersen, J., Nowak, W., Gayler, S., Streck, T., 2022. Combining crop modeling with remote sensing data using a particle filtering technique to produce real-time forecasts of winter wheat yields under uncertain boundary conditions. Remote Sens. 14 (6).

Zhang, C., Xie, Z., Wang, Q., Tang, M., Feng, S., Cai, H., 2022. AquaCrop modeling to explore optimal irrigation of winter wheat for improving grain yield and water productivity. Agric. Water Manag. 266.

Zhang, G., Zhang, Z., Li, X., Zheng, B., Zhang, X., 2023. EvolutioN Characteristics of Meteorological Drought under Future Climate Change in the Middle Reaches of the Yellow River Basin based on the copula function. Water 15 (12).

Zhu, H., Jiang, Z., Li, L., 2021. Projection of climate extremes in China, an incremental exercise from CMIP5 to CMIP6. Sci. Bull. 66 (24), 2528–2537.

Zhu, H., Jiang, Z., Li, J., Li, W., Sun, C., Li, L., 2020. Does CMIP6 inspire more confidence in simulating climate extremes over China? Adv. Atmos. Sci. 37 (10), 1119–1132.